Hindawi
Mathematical Problems in Engineering
Volume 2018, Article ID 7012710, 10 pages
https://doi.org/10.1155/2018/7012710

Research Article

Mechanism Analysis of Spalling Defect on Rail Surface under Rolling Contact Conditions

Rongshan Yang,[1] Shihao Cao ,[2] Weixin Kang,[1] Jiali Li,[1] and Xiaoyu Jiang[3]

[1]*MOE Key Laboratory of High-Speed Railway Engineering, Southwest Jiaotong University, Chengdu 610031, China*
[2]*College of Civil Engineering and Architecture, Henan University of Technology, Zhengzhou 450001, China*
[3]*College of Mechanics and Engineering, Southwest Jiaotong University, Chengdu 610031, China*

Correspondence should be addressed to Shihao Cao; 531148108@qq.com

Received 9 October 2017; Accepted 24 January 2018; Published 21 February 2018

Academic Editor: Fabrizio Greco

Under the wheel/rail contact loading conditions, the microcracks on the rail surface propagate, leading to spalling defect or rail fracture and threatening the travelling safety of high-speed railway directly. In order to analyze the mechanism of the crack propagation on the rail surface, the calculation model of the wheel/rail contact fatigue was established, and the variation of the stress intensity factor at the crack tip when the crack length was increased from 0.1 mm to 2 mm was obtained. Based on the mixed-mode fracture criterion and Paris growth theory, the mechanism of the crack propagation on the rail surface was analyzed. The results show that when the microcrack grows to macrocrack, the mode of the fatigue crack on the rail surface is mixed including sliding mode and open mode. With the increase of the crack length, the stress intensity factor K_{I} increases first and then decreases gradually, and the relative dangerous location of the open-mode crack moves from the inner edge of the contact area to the outer edge, while the factor K_{II} is increasing during the whole propagation process, and the relative dangerous location of the sliding-mode crack remains unchanged basically. The main failure mode of crack is open during the initial stage and then transforms into sliding mode with the crack length increasing. The crack tends to propagate upward and leads to spalling defect when the crack length is between 0.3 and 0.5 mm. This propagation path is basically identical with the spalling path of the service rail. The research results will provide a basis for improving the antifatigue performance of rail and establishing the grinding procedure.

1. Introduction

As the travelling base of the high-speed railway, rail plays a role of supporting and guiding the running of the train. However, due to the repeated extrusion caused by the contact stress between the wheel and the rail, microcrack initiation and propagation will appear on the surface of the rail. As a result, there will be rail head spalling or even fracture. With the freight volume and the train speed increasing, rolling contact fatigue (RCF) has become more and more serious, which affects the traffic safety directly [1]. For example, in 2000, a serious derailment accident happened to a British high-speed train because of the fractured rail [2]. Coincidentally, there were also rail fractures caused by the two oblique cracks in the Guangzhou-Shenzhen high-speed railway in 2002 [3].

Many researches about the growth path of the wheel/rail contact fatigue have been reported. The review by Smith et al. [2, 4] indicated that there was an acute angle between the crack initiation and the direction of train running during the initial stage, and the growth angle increased with the increase of the depth, and, finally, the rail fractured in the direction perpendicular to the surface, as shown in Figure 1(a). Chen et al. [5] studied the spalling path of the rail head through slice analysis and concluded that when the cracks grew to a certain depth, they would change their propagation direction and then spread approximately along the right-about with train running direction towards the rail surface; consequently, spalling was formed in the shape of barb, as shown in Figure 1(b). Through analyzing the chemical composition and mechanical properties of rail with spalling defects, Zhou et al. [6] proposed that the generation of spalling defects had no

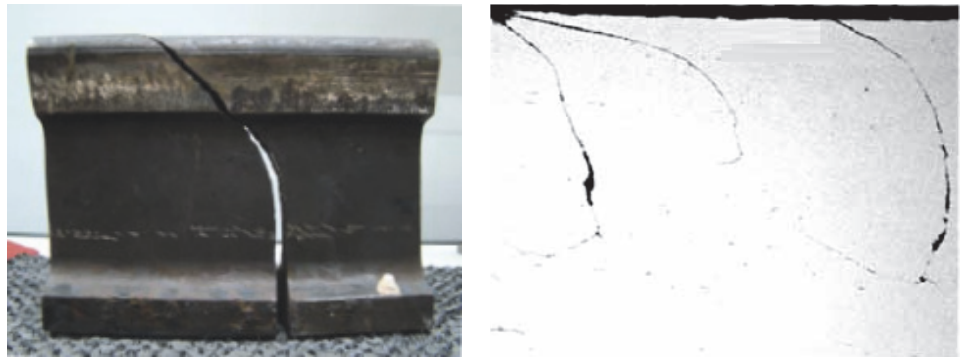

(a) (b)

Figure 1: Growth path of the rolling contact fatigue cracks: (a) fracture and (b) spalling on the rail surface.

direct relation with the rail quality, which was mainly caused by the excessive contact stress.

In the aspect of experimental study, through the convex-concave contact configuration of a shaft running inside a ring, Christoph et al. [7] performed a laboratory test simulating the fatigue inclined cracks on the rail surface. Huang et al. [8, 9] characterized the wear of the rail surface via WR-1 wheel/rail rolling wear testing apparatus. Based on the field observation of rolling contact fatigue, Tao [10] investigated the cause of wheel tread spalling preliminarily by the use of shakedown theory.

With respect to the mechanism of microcracks initiation, Langueh et al. [11, 12] proposed that stress concentration in the local region was the main cause of fatigue cracks initiation under the action of the contact stress. Dubourg et al. [13, 14] argued that shear stress played a significant role in the initiation of cracks. Jiang and Jin [15, 16] proposed that the large residual tensile stress on the rail surface could possibly be an important factor of microcracks initiation. As for the crack propagation mechanism, Ringsberg et al. [17–19] studied the microcracks propagation mechanism of the rail surface based on the Hertz theory and the wheel/rail tribology and found that the propagation of microcracks on surface was mainly open mode. With regard to the long cracks, Seo et al. [4, 20, 21] investigated that sliding propagation was their major mode, and their propagation rate increased as the friction coefficient between the wheel and the rail increased.

Currently, most studies about the propagation mechanism of cracks are focused on macro long cracks, which ignore the stage when microcrack transforms into macrocrack. In fact, this stage is the main part of the entire propagation process, and most rail spalling occurs in this stage as well [10]. Therefore, based on the assumption that the wheel was rolling along the rail, this paper analyzed the propagation characteristics of the fatigue cracks on the rail surface from microcrack to macrocrack and made the fatigue spalling mechanism of rails more clear, which could provide the basis for the improvement of the rail fatigue performance and the establishment of grinding procedure. In this way the operation costs as well as risks will be cut down.

2. Force Analysis of Wheel/Rail Contact

With the development of production technology in rails, it is hard to find rolling contact fatigue (RCF) defects caused by nonmetallic inclusions in rail and hydrogen induced crack. However, in the high-speed passenger dedicated lines and heavy haul lines, the RCF defects that occurred on the rail head surface become more and more serious, these defects are mainly caused by the huge contact stress act on the rail surface [6].

2.1. Hertz Contact Theory. As the theoretical basis of calculating the wheel/rail contact stress, the Hertz contact theory assumes that the wheel/rail contact area is an ellipse, and the maximum contact pressure $q_{\max}$ is in the center of the ellipse, which is given by [18].

$$q_{\max} = \frac{3P}{2\pi ab}, \tag{1}$$

where P is the force act on the rail and a is the semimajor axis of the elliptical contact area, while b is the semiminor axis of the elliptical contact area. Then the values of a and b can be obtained by

$$a = m\sqrt[3]{\frac{3\left(1-\upsilon^2\right)P}{2E\left(A+B\right)}}$$
$$b = \frac{n}{m}a, \tag{2}$$

where E is Young's modulus and υ is Poisson's ratio, while m and n denote the calculating coefficients of wheel/rail contact stress [22].

As for the coefficients A and B, they can be obtained through

$$A + B = \frac{1}{2}\left(\frac{1}{R_1} + \frac{1}{R_2}\right)$$
$$B - A = \frac{1}{2}\left(\frac{1}{R_1} - \frac{1}{R_2}\right), \tag{3}$$

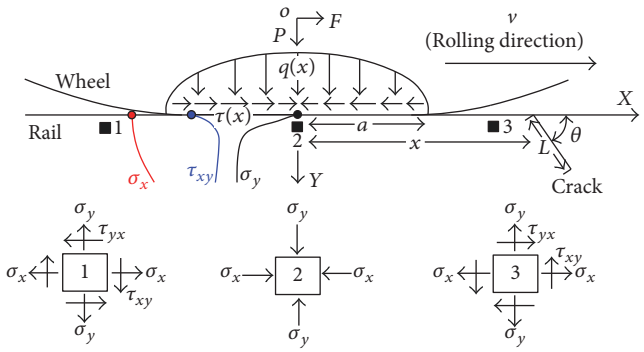

Figure 2: Distribution of contact forces and stress state of rail surface under the action of rolling wheel.

where R_1 is the radius of the wheel, R_2 is the crown radius of the rail head.

The distribution of the contact pressure acting on the rail is

$$q(x) = q_{\max}\sqrt{1-\frac{x^2}{a^2}}, \tag{4}$$

The tangential friction force in the contact area can be obtained according to Coulomb's law of friction [23]. When the wheel-rail contact is in an adhesion condition, the tangential friction force is described as

$$\tau(x) \le \mu q(x). \tag{5}$$

When the contact is in a sliding condition, the tangential friction force is

$$\tau(x) = \mu q(x), \tag{6}$$

where $\tau(x)$ is the tangential friction force in the contact area and μ is the friction coefficient of wheel and rail.

See Figure 2, where X is the longitudinal direction of the rail, Y is the depth direction of the rail, a is the semimajor axis of the contact area, x is the distance from the center of the contact area to the crack, P is the force act on the rail, v is the rolling direction of the wheel, L is the crack length, θ is the angle between crack and rolling direction, σ_x is the horizontal normal stress of the rail surface, σ_y is the vertical normal stress of the rail surface, and τ_{xy} is the shear stress of the rail surface. And the numbers 1, 2, and 3 denote the rail microelements bearing the forces when the wheel is close to different positions, respectively.

2.2. Stress State of the Rail Surface. When a wheel is rolling along the rail, the area of the contact area is approximately 100 mm^2, and the load act on the contact area is about 50~200 kN, which could result in a huge contact stress [24]. Under the action of the normal contact pressure and the tangential friction force, the stress state of the rail surface can be seen from Figure 2. When the wheel rolls from position 1 to position 3, the horizontal tensile stress and shear stress will have periodic changes in direction. In general, this combined alternating stress is considered to be the main cause of the crack initiation and propagation on the rail surface.

Table 1: Mechanical properties of steel (U71Mn).

Type of rail	Young's modulus/GPa	Poisson's ratio	Yield strength/MPa	Tangent modulus/GPa
U71Mn steel	210	0.3	550	21

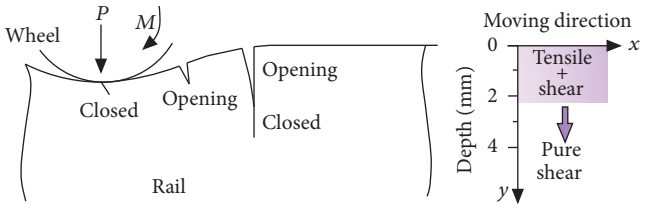

Figure 3: State of crack on the rail surface.

2.3. Analysis of the Crack State. When the wheel is close to or away from the crack, the extrusion effect on the rail surface leads to the stretch of the surface material near the edges of the contact area. At the same time, the surface cracks of the rail will open under the action of tensile stress. While the wheel pressure acts on the crack, the crack will be closed because of the mutual extrusion of the crack surfaces, as shown in Figure 3.

3. Calculation Model and Methods of the Wheel/Rail Contact Fatigue

3.1. Calculation Model and Parameters. The type of the rail is 60 kg/m (U71Mn), whose mechanical properties are listed in Table 1 [18]. The model is 176 mm in height and 600 mm in length. There is an angle of 60° between the crack and the rail surface, and the crack length varies from 0 to 2 mm. Without considering the influence of the foundation, the fixed constraint is applied at the bottom of the model. In order to describe the singularity of the crack tip, the singular element (PLANE 183) with eight nodes is adopted, and quarter-points singular degenerated elements are used to model the stress singularity around the crack tip. Then the finite element model for the whole rail and the local model at the crack tip are presented in Figure 4.

3.2. Calculation Principle of the Stress Intensity Factor K. Based on the displacement extrapolation method, the stress intensity factor (K) at the crack tip can be calculated by the finite element software ANSYS [25–27]. The reference coordinate system is shown in Figure 5, and the relationship between the displacement of the nodes near the crack tip and the stress intensity factor is described as

$$u = \frac{K_{\mathrm{I}}}{4G}\sqrt{\frac{r}{2\pi}}\left((2\kappa-1)\cos\frac{\theta}{2}-\cos\frac{3\theta}{2}\right) + \frac{K_{\mathrm{II}}}{4G}\sqrt{\frac{r}{2\pi}}\left((2\kappa+3)\sin\frac{\theta}{2}+\sin\frac{3\theta}{2}\right)+o(r)$$

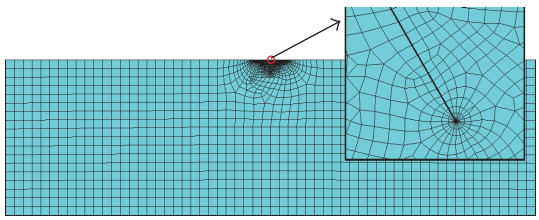

Figure 4: Finite element model of rail with crack on the surface.

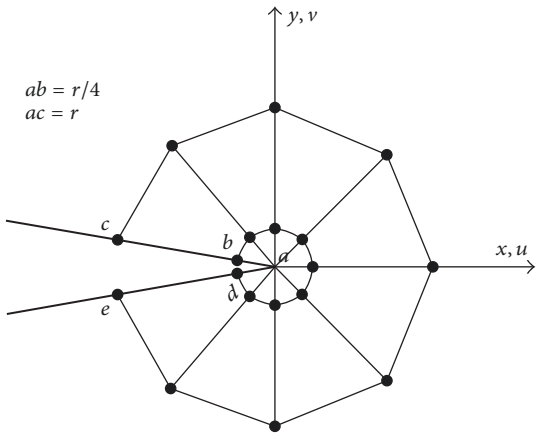

Figure 5: Singular elements at the crack tip and their coordinates.

$$v = \frac{K_{\mathrm{I}}}{4G}\sqrt{\frac{r}{2\pi}}\left((2\kappa+1)\sin\frac{\theta}{2} - \sin\frac{3\theta}{2}\right) - \frac{K_{\mathrm{II}}}{4G}\sqrt{\frac{r}{2\pi}}\left((2\kappa-3)\cos\frac{\theta}{2} + \cos\frac{3\theta}{2}\right) + o(r), \tag{7}$$

where u and v are the displacement components in the x and y directions, respectively. G is the shear modulus and K is the stress intensity factor, while κ is the coefficient related to Poisson's ratio, and their relationship is shown in

$$\kappa = \begin{cases} \dfrac{(3-\mu)}{(1+\mu)} & \text{for plane stress} \\ 3-4\mu & \text{for plane strain,} \end{cases} \tag{8}$$

where μ is Poisson's ratio.

When the angle θ equals $\pm 180^{\circ}$, (7) can be simplified to

$$K_{\mathrm{I}} = \frac{G(v_c - v_e)}{\kappa+1}\sqrt{\frac{2\pi}{r}}$$
$$K_{\mathrm{II}} = \frac{G(u_c - u_e)}{\kappa+1}\sqrt{\frac{2\pi}{r}}. \tag{9}$$

Equation (9) can be used to evaluate the stress intensity factor K at the crack tip.

4. Calculation Results and Analysis

4.1. The Relative Dangerous Position of the Cracks. While the wheels of different axle load (10, 15, and 20 t) are rolling along the rail surface with cracks, the variation trends of the stress intensity factors (K_{I} and K_{II}) at the tip of cracks with different lengths (i.e., 0.1, 0.2, 0.3, 0.4, 0.5, 0.7, 1, 1.5, and 2 mm) are shown in Figure 6, where x denotes the distance from the center of the contact area to the crack.

According to Figures 6(a), 6(c), and 6(e), it is easy to find that, with the increase of the crack length, both the maximum value of K_{I} and its position are changing. Under the condition that the axle load is 10 t, if the crack length is less than or equal to 0.2 mm, the inner edge of the contact area has the maximum value of K_{I}. While the crack length is larger than 0.2 mm, there is the maximum value of K_{I} at the outer edge of the contact area. And when the axle load is increased to 15 t, the maximum value of K_{I} will occur at the inner edge of the contact area if the crack length is less than or equal to 0.5 mm. Similarly, when the crack length is larger than 0.5 mm, the outer edge of the contact area will have the maximum value of K_{I}. When the axle load is 20 t, if the crack length is less than or equal to 0.7 mm, the inner edge of the contact area has the maximum value of K_{I}. When the crack length is larger than 0.7 mm, there is the maximum value of K_{I} at the outer edge of contact area, where the corresponding semilength values of the contact area for different axle load (10, 15, and 20 t) are 5.9, 7, and 8 mm, respectively. The results indicate that, with the increase of the crack length, the critical position where the crack has open failure is changed from the inner edge of the contact area to the outer edge.

Figures 6(b), 6(d), and 6(f) illustrate that, compared with K_{I}, the maximum value of K_{II} mainly occurs at the inner edge of the contact area. When the axle load is 10 t, the maximum value of K_{II} varies between 4.45 and 4.75 mm. When the axle load is increased to 15 t, the maximum value of K_{II} changes between 5.5 and 6.1 mm, while, under the axle load of 20 t, the maximum value of K_{II} is changing between 6.4 and 6.6 mm. What is more, with the increase of the crack length, the position where the maximum value of K_{II} occurs will be closer to the center of the contact area slightly.

4.2. Governing Factors of the Crack Propagation. Under the different axle load of 10 t, 15 t, and 20 t, the variation trends of the maximum stress intensity factors ($K_{\mathrm{I\,max}}$ and $K_{\mathrm{II\,max}}$) at the crack tip are shown in Figure 7.

As seen in Figure 7, with the increase of the crack length, the value of $K_{\mathrm{I\,max}}$ has a sharp increase at the beginning and then decreases gradually. When the crack length is 0.3 mm, the factor $K_{\mathrm{I\,max}}$ has the maximum value. The possible explanation can be given by the distribution of the longitudinal stress (σ_x) on the rail surface, as shown in Figure 8(a). The maximum tensile stress occurs at the rail surface, and, with the increase of the depth, the tensile stress decreases significantly. While the depth exceeds a critical value, the rail will be in compression and the crack closure occurs. As for the factor $K_{\mathrm{II\,max}}$, with the increase of the crack length, the value of $K_{\mathrm{II\,max}}$ also has a sharp increase first, and

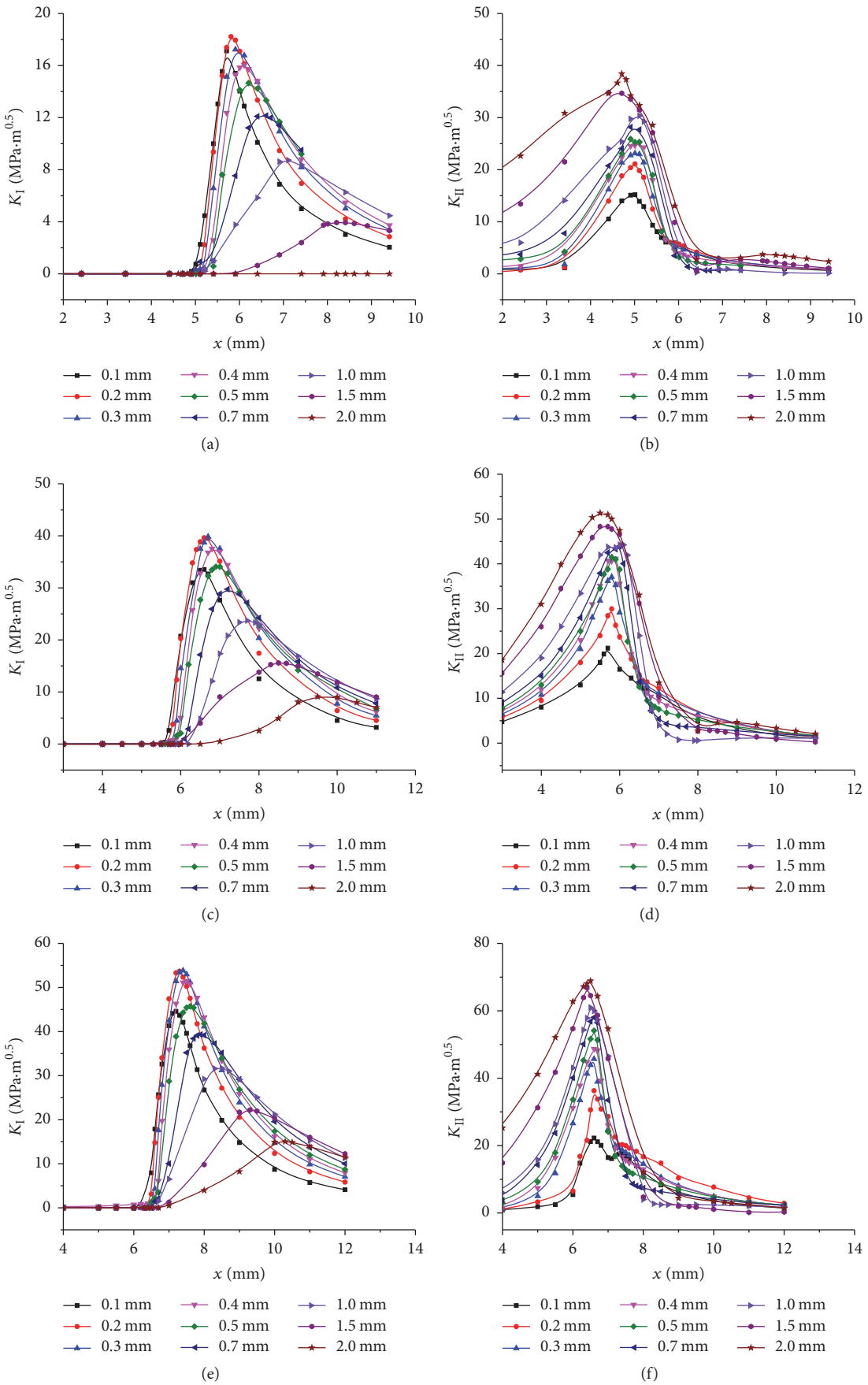

Figure 6: Position relationship between the stress intensity factors (K_I and K_{II}) and the contact area: (a) K_I—10 t; (b) K_{II}—10 t; (c) K_I—15 t; (d) K_{II}—15 t; (e) K_I—20 t; (f) K_{II}—20 t.

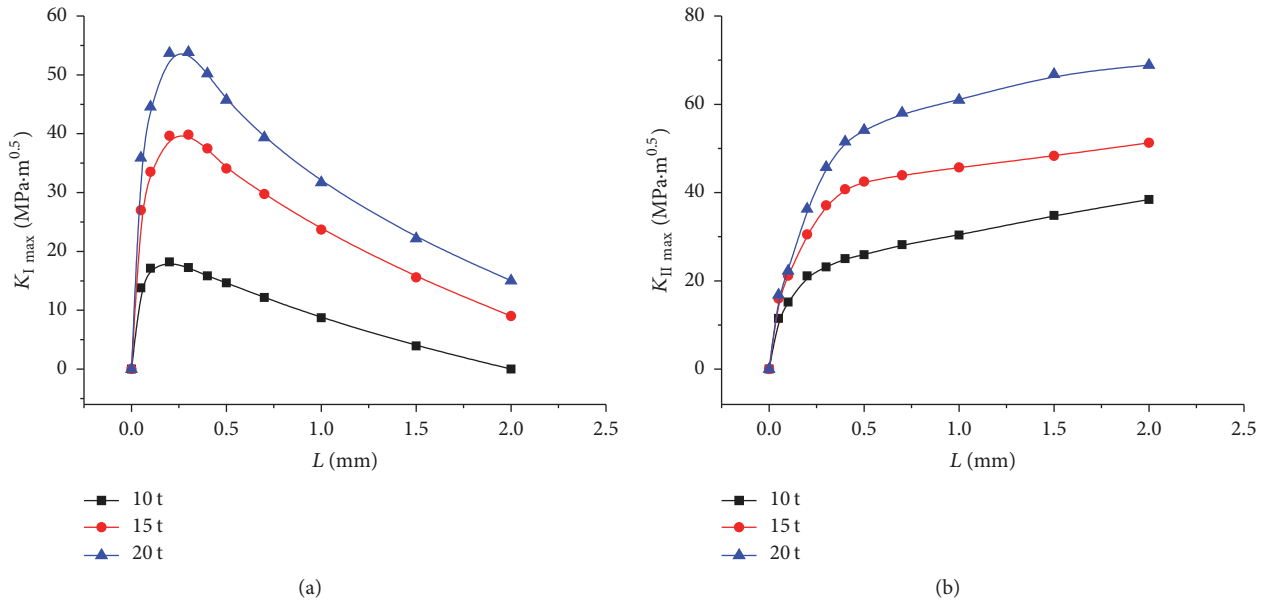

FIGURE 7: Variations of $K_{I\,max}$ and $K_{II\,max}$ with the increase of the crack length: (a) $K_{I\,max}$ and (b) $K_{II\,max}$.

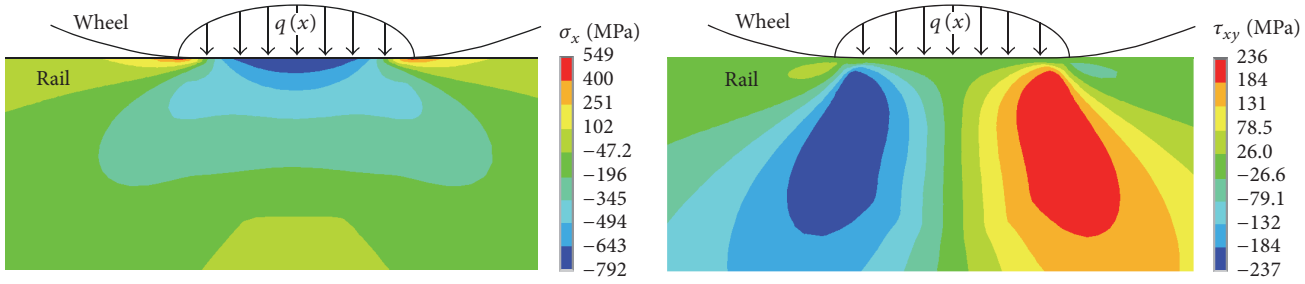

FIGURE 8: Stress contour of the rail surface (the axle load is 15 t): (a) σ_x and (b) τ_{xy}.

then its increase rate tends to be slow. The reason can be found from the shear stress distribution on the rail surface, with respect to the tensile stress caused by the wheel/rail contact, the maximum shear stress mainly occurs at a certain depth which is below the rail surface. When the axle load is 15 t, the maximum shear stress occurs at the edge of the contact area which is about 4 mm below the surface, as shown in Figure 8(b).

To sum up, the rolling contact fatigue crack belongs to mixed-mode crack with open mode (I) as well as sliding mode (II). Furthermore, as for different length of the cracks, their governing factors of crack growth are not always the same. When the crack length is less than 0.3 mm, the fatigue crack is mainly open mode. While the crack length is larger than 0.3 mm, the sliding mode takes the leading role. And when the crack increases to a certain length, the crack tip tends to close, and K_I is equal to zero. At the moment, the fatigue crack on the rail surface becomes pure sliding mode (II) without being open.

4.3. Propagation Rate of the Cracks. Since the wheel/rail contact fatigue crack belongs to mixed-mode crack (I and II), it is necessary to adopt the equivalent stress intensity factor K_{eff} to exhibit the combined effect of the factors (K_I and K_{II}), as shown in [28]

$$K_{eff} = K_I + K_{II}, \tag{10}$$

where K_I and K_{II} are stress intensity factors, which denote the open failure and sliding failure mode, respectively.

The propagation rate of the crack can be obtained by the Paris-Erdogan model, as shown in [29, 30]

$$\frac{da}{dN} = C(\Delta K)^m, \tag{11}$$

where da/dN is the crack growth per cycle and C and m are material constants to be found experimentally, while ΔK is the stress intensity factor range, which can be determined by

$$\Delta K = K_{max} - K_{min}, \tag{12}$$

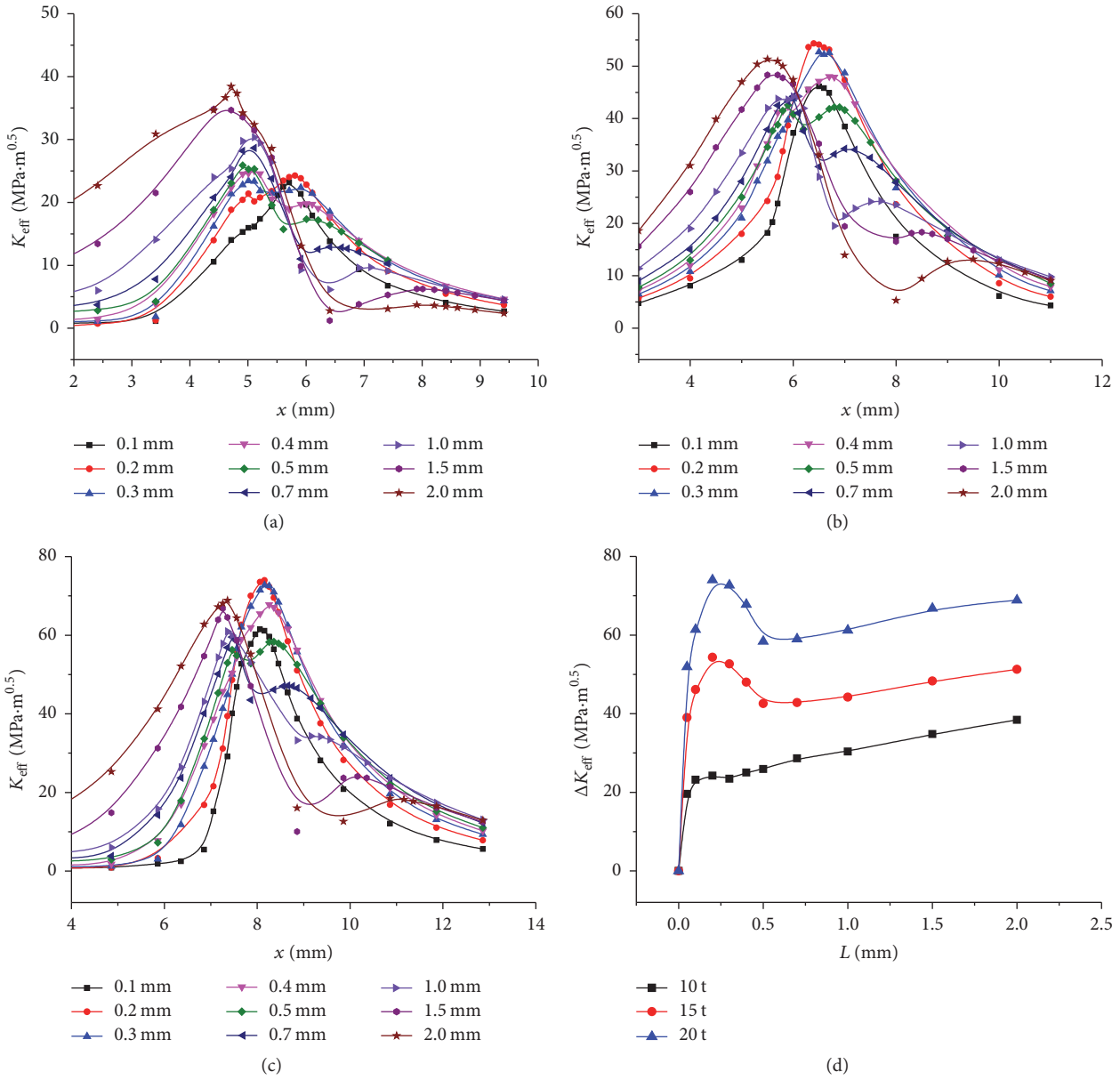

FIGURE 9: Variations of K_{eff} and ΔK_{eff} for different crack length: (a) K_{eff}—10 t; (b) K_{eff}—15 t; (c) K_{eff}—20 t; and (d) ΔK_{eff}.

where K_{max} is the maximum value of stress intensity factor K and K_{min} is the minimum value of stress intensity factor K.

When different axle load of the wheels (i.e. 10, 15, and 20 t) is rolling along the rail surface with cracks, the variation trends of the equivalent intensity factors K_{eff} and their ranges ΔK_{eff} for different crack length are illustrated in Figure 9.

According to Figures 9(a), 9(b), and 9(c), it is clear that different length of the cracks all have two peak values of the equivalent stress intensity factor (K_{eff}), and the distance between the two peaks increases with the increase of the crack length. The peak near the center of the contact area is mainly governed by the factor K_{II}, while the peak far away from the center of the contact area is mainly controlled by the factor K_I.

From Figure 9(d), it can be concluded that the equivalent stress intensity range ΔK_{eff} has a sharp increase as the crack length increases. When the crack length is about 0.3 mm, there will be the first peak of ΔK_{eff} occurring, and then it decreases. When the crack length is larger than 0.5 mm, the factor range increases again. That is to say, when the crack length is between 0.3 and 0.5 mm, because the rate the crack grows to a certain depth of the rail is less compared to growing to the rail surface, therefore, during this phase, the crack tends to grow towards the rail surface, and then the rail spalling occurs. This spalling path of the rail surface has a good

Table 2: Predicted propagation angles of the cracks based on the maximum circle tensile stress criterion.

Crack length /mm	Axle load /t	K_{eff}/MPa·m$^{0.5}$	K_I/MPa·m$^{0.5}$	K_{II}/MPa·m$^{0.5}$	Initial angle of the crack/°	Turning angle of the crack/°	Propagation angle of the crack/°
0.3	10	23.44	0.31	23.13	60	70.78	130.78
0.4	10	25.04	0.00	25.04	60	70.53	130.53
0.5	10	25.91	0.00	25.91	60	70.53	130.53
0.3	15	52.69	37.51	15.18	60	114.57	174.57
0.4	15	48.03	36.79	11.24	60	124.49	184.49
0.5	15	42.58	1.61	40.97	60	71.28	131.28
0.3	20	72.73	53.46	19.27	60	118.60	178.60
0.4	20	67.78	51.14	16.64	60	122.23	182.23
0.5	20	58.36	45.44	12.92	60	127.06	187.06

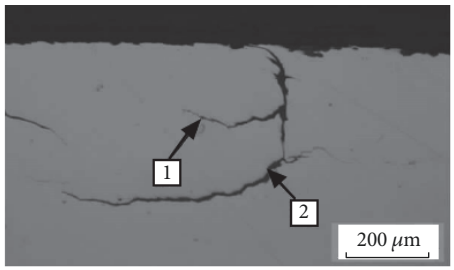

Figure 10: Typical surface spalling path of the service rail.

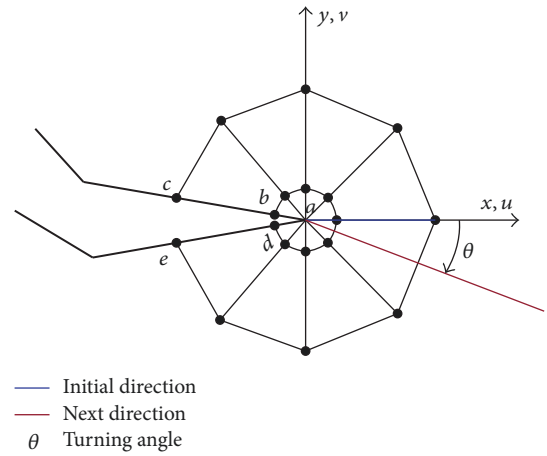

Figure 11: Turning direction of the crack based on the maximum circle tensile stress criterion.

agreement with the field observation, as shown in Figure 10 [31].

4.4. Angles of the Crack Propagation. With respect to the mixed-mode crack (I and II), the propagation direction of the crack is not always the same. However, it tends to grow in the direction in which the maximum circle tensile stress occurs [32]. According to this criterion, the turning angle of the crack propagation can be obtained, as described in

$$\theta = 2\tan^{-1}\left[\frac{1}{4}\frac{K_I}{K_{II}} + \frac{1}{4}\sqrt{\left(\frac{K_I}{K_{II}}\right)^2 + 8}\right], \quad (13)$$

where θ is the turning angle of the crack and its turning direction is illustrated in Figure 11.

When the crack length is between 0.3 and 0.5 mm, the crack may turn to grow towards the rail surface in an opposite direction. Aimed at analyzing the reasons why the rail spalling is formed in the shape of barb, based on the maximum circle tensile stress criterion, the propagation directions of the cracks with different length (0.3, 0.4, and 0.5 mm) are predicted under different axle loading (10, 15, and 20 t). The calculation results are listed in Table 2 and Figure 12.

As is illustrated in Figure 12, it can be found that when the axle load is 10 t, although the propagation direction of the crack has a certain turning, its general propagation tends downward, which is likely to fracture. While the axle load is 15 t or 20 t, the propagation direction will have a change and grow towards the rail surface. As a result, the spalling is formed in the shape of barb. In addition, according to Figures 12(b) and 12(c), compared with an axle load of 15 t, the crack is more likely to propagate towards the rail surface when the axle load is 20 t. This phenomenon may explain why the spalling of rail surface occurs more frequently in the line of heavy haul [5, 6, 31].

5. Conclusions

In this paper, in order to analyze the mechanism of the crack propagation on the rail surface, the calculation model of the wheel/rail contact fatigue was established, and the variation of the stress intensity factor at the crack tip when the crack length was increased from 0.1 mm to 2 mm was obtained. Based on the mixed-mode fracture criterion and Paris growth theory, the mechanism of the crack propagation on the rail surface was analyzed. The research results will provide a basis for improving the antifatigue performance of rail and establishing the grinding procedure. And the following conclusions can be drawn:

(1) In the process when the microcrack grows to macrocrack, the mode of the fatigue crack on the rail surface

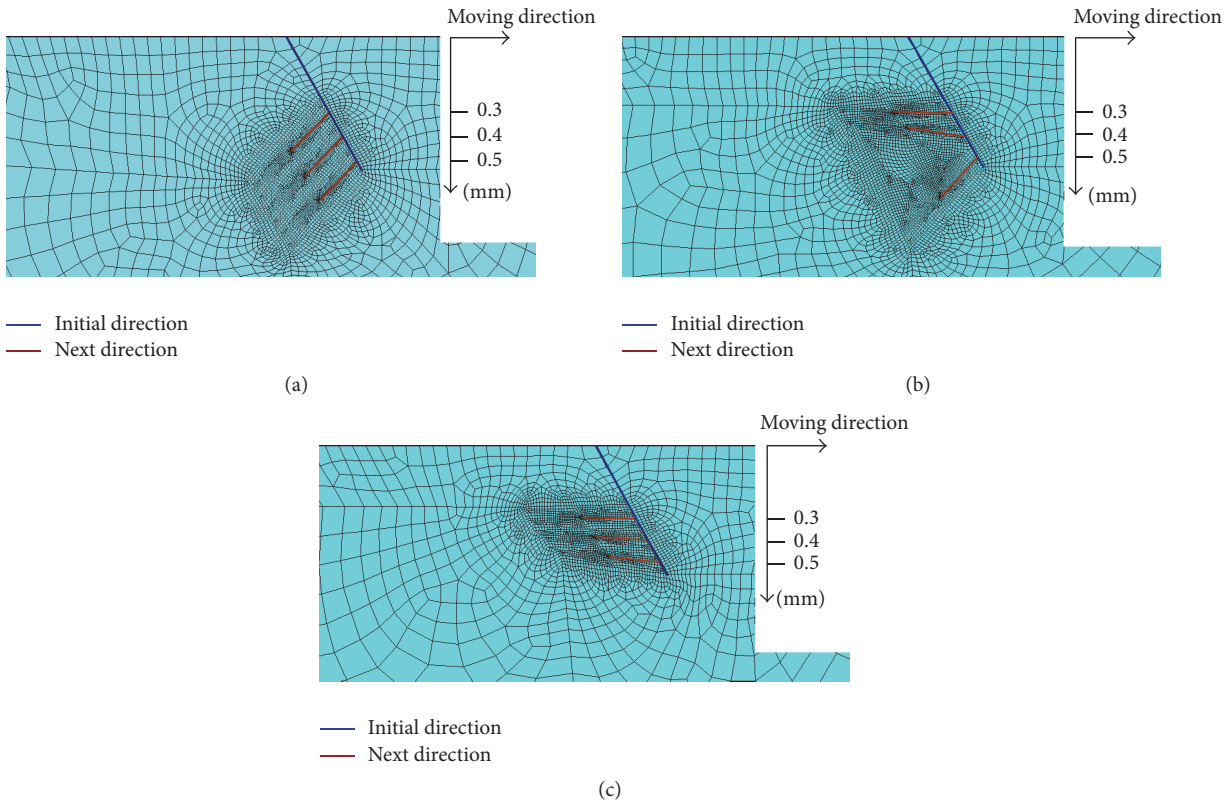

Figure 12: Predicted propagation paths of the crack based on the maximum circle tensile stress criterion: (a) 10 t; (b) 15 t; and (c) 20 t.

is mixed including open mode and sliding mode. And, with the increase of the crack length, the main propagation mode of the fatigue crack changes from open mode to sliding mode.

(2) With the increase of the crack length, the stress intensity factor K_I increases rapidly and then decreases gradually, the relatively dangerous location of open-mode crack moves from the inner edge of the contact area to the outer edge. While the factor K_{II} increases during the whole propagation process, and the relative dangerous location of sliding-mode crack remains the same roughly.

(3) The crack tends to propagate upward and leads to spalling defect when the crack length is between 0.3 and 0.5 mm. The propagation path is basically identical with the spalling path of the service rail in the field.

Conflicts of Interest

The authors declare that they have no conflicts of interest.

Acknowledgments

Financial support for the research was provided by the National Natural Science Foundation of China (no. 11472230, no. 51778543) and the Key Project of National Natural Science Foundation of China (no. U1434208).

References

[1] D. X. Yang, "Research on development direction of track technology of heavy-haul railway," *Journal of Railway Engineering Society*, vol. 161, pp. 41–44, 2012.

[2] R. A. Smith, "Rolling contact fatigue of rails: what remains to be done," *China Railway Science*, vol. 23, no. 3, pp. 6–10, 2002.

[3] Guangzhou Railway Company of Public Works, *Exchange Data of Rail Damage Seminar of Guangshen Lion*, Guangzhou Railway Company, 2003.

[4] J. Seo, S. Kwon, H. Jun, and D. Lee, "Fatigue crack growth behavior of surface crack in rails," *Procedia Engineering*, vol. 21, no. 1, pp. 865–872, 2010.

[5] Z. Y. Chen, Y. H. Zhang, F. S. Liu, and Q. Zhou, "Analysis on the formation cause of spalling and damage of the heat-treated low rail on Shuohuang railway curve," *China Railway Science*, vol. 29, no. 4, pp. 28–34, 2008.

[6] J. H. Zhou, A. C. Ren, Y. Ji et al., "Analysis of the reasons for the spalling defects on U71Mn rail treads," *China Railway Science*, vol. 34, no. 3, pp. 1–6, 2003.

[7] K. Christoph, H. Anton, and P. Reinhard, "A novel laboratory test rig for probing the sensitivity of rail steels to RCF and wear-first experimental results," *Wear*, vol. 316, no. 1, pp. 101–108, 2014.

[8] Y. B. Huang, C. G. He, L. Ma et al., "Experimental study on initiation of surface fatigue crack of wheel material under dry condition," *Tribology*, vol. 36, no. 2, pp. 194–200, 2006.

[9] L. Ma, C. G. He, X. J. Zhao et al., "Study on wear and rolling contact fatigue behaviors of wheel/rail materials under different slip ratio conditions," *Wear*, vol. 366-367, pp. 13–26, 2016.

[10] G. C. Tao, *Preliminary study on the cause of wheel tread shelling of KKD [M.S. thesis]*, Southwest Jiaotong University, 2013.

[11] A. M. G. Langueh, J.-F. Brunel, E. Charkaluk, P. Dufrénoy, J.-B. Tritsch, and F. Demilly, "Effects of sliding on rolling contact fatigue of railway wheels," *Fatigue & Fracture of Engineering Materials & Structures*, vol. 36, no. 6, pp. 515–525, 2013.

[12] M. D. Sangid, "The physics of fatigue crack initiation," *International Journal of Fatigue*, vol. 57, pp. 58–72, 2013.

[13] M. C. Dubourg and B. Villechaise, "Analysis of multiple fatigue cracks-part I: theory," *Journal of Tribology*, vol. 114, no. 3, pp. 455–461, 1992.

[14] M. C. Dubourg, M. Godet, and B. Villechaise, "Analysis of multiple fatigue cracks-part II: results," *Journal of Tribology*, vol. 114, no. 3, pp. 462–468, 1992.

[15] X. Y. Jiang and X. S. Jin, "Elastic-Plastic analysis of contact problems of wheel/rail with surface micro-roughness," *Journal of Southwest Jiaotong University*, vol. 36, no. 6, pp. 588–590, 2001.

[16] X. Y. Jiang and X. S. Jin, "Influence of liquid and micro-roughness on the fatigue of wheel/rail contact," *Journal of Mechanical Engineering*, vol. 40, no. 8, pp. 18–23, 2004.

[17] J. W. Ringsberg, "Shear mode growth of short surface-breaking RCF cracks," *Wear*, vol. 258, no. 7-8, pp. 955–963, 2005.

[18] S. H. Cao, X. Li, S. F. Zhang, L. Wen, and X. Jiang, "Research of the differences between Hertz theory and finite element method to analyze the fatigue of wheel/rail contact," *Journal of Mechanical Engineering*, vol. 51, no. 6, pp. 126–134, 2015.

[19] K. J. Miller, "The short crack problem," *Fatigue & Fracture of Engineering Materials & Structures*, vol. 5, no. 3, pp. 223–232, 1982.

[20] Y. G. Deng, W. Li, Z. F. Wen et al., "Analysis of crack propagation on rail weld surface under wheel/rail interaction," *Chinese Journal of Applied Mechanics*, vol. 30, no. 4, pp. 624–629, 2013.

[21] X. Li, S. H. Cao, L. H. Wen et al., "The influence of crack length on the propagation of rail crack," *Applied Mathematics and Mechanics*, vol. 35, supplement 1, pp. 131–135, 2014.

[22] S. H. Cao, *The propagation and prevention of fatigue cracks on rail surface [M.S. thesis]*, Southwest Jiaotong University, 2014.

[23] X. Jiang and X. Jin, "Numerical simulation of wheel rolling over rail at high-speeds," *Wear*, no. 262, pp. 666–671, 2007.

[24] X. S. Jin, X. S. Zhang, and J. Zhang, "Mechanics in performance of wheel/rail," *Journal of Mechanical Strength*, vol. 27, no. 4, pp. 408–418, 2005.

[25] R. S. Barsoum, "On the use of isoparametric finite elements in linear fracture mechanics," *International Journal for Numerical Methods in Engineering*, vol. 10, no. 1, pp. 25–37, 1976.

[26] D. M. Tracey, "Discussion of 'on the use of isoparametric finite elements in linear fracture mechanics' by R. S. Barsoum," *International Journal for Numerical Methods in Engineering*, vol. 11, no. 2, pp. 401-402, 1977.

[27] J. M. Alegre and I. I. Cuesta, "Some aspects about the crack growth FEM simulations under mixed-mode loading," *International Journal of Fatigue*, vol. 32, no. 7, pp. 1090–1095, 2010.

[28] Q. F. Li, *Fracture Mechanics and Engineering Applications*, Harbin Engineering University Press, 2007.

[29] R. M. Nejad, M. Shariati, and K. Farhangdoost, "Effect of wear on rolling contact fatigue crack growth in rails," *Tribology International*, vol. 94, pp. 118–125, 2016.

[30] H.-K. Jun, J.-W. Seo, I.-S. Jeon, S.-H. Lee, and Y.-S. Chang, "Fracture and fatigue crack growth analyses on a weld-repaired railway rail," *Engineering Failure Analysis*, vol. 59, pp. 478–492, 2016.

[31] H. M. Guo, W. J. Wang, T. F. Liu et al., "Analysis of damage behavior of heavy-haul railway rails," *China Mechanical Engineering*, vol. 25, no. 2, pp. 267–272, 2014.

[32] F. Erdogan and G. C. Sih, "On the crack extension in plates under plane loading and transverse shear," *Journal of Basic Engineering*, vol. 85, no. 4, pp. 519–525, 1963.